Fault Analysis of a Non-Isolated Three-Level DC-DC Converter Integrated in a Bipolar DC Power Grid

Catia F. Oliveira, Joao L. Afonso, Vitor Monteiro

ALGORITMI Research Centre, University of Minho, Guimarães, Portugal
{c.oliveira,jla,vmonteiro}@dei.uminho.pt
c.oliveira@dei.uminho.pt

Abstract. DC power grids present significant advantages over AC power grids, namely higher stability and controllability, and the absence of harmonic currents and reactive power. Moreover, DC grids facilitate the interface with renewable energy sources (RES) and energy storage systems (ESS). DC grids can be either unipolar or bipolar, where the latter consists of three wires and provides higher flexibility, reliability and transmission capacity. However, failures in bipolar DC grids (especially in the power semiconductors) can occur. The consequences of these failures can result in increased costs, depending on the damage, e.g., if it occurs a wire of the DC grid or in the connected power converter. Thus, in this paper is presented a fault analysis of a non-isolated three-level DC-DC converter used to interface solar photovoltaic (PV) panels into a bipolar DC power grid. The fault analysis is conceived through computational simulations, where can be observed the performance of the presented DC-DC converter under fault conditions in each wire of the bipolar DC grid. The simulation results demonstrate the DC-DC converter operating in two different situations: steady-state and transient-state. The control strategy applied in normal and fault conditions, as well as the different operation modes, are explained in detail.

Keywords: Bipolar DC Power Grid; Three-level DC-DC Converter; Solar PV Panels; Fault Analysis.

1 Introduction

The increasing emission of greenhouse gases caused by industrialization and transport sector requires the development of viable solutions to mitigate environment degradation [1]. In view of this, the integration of renewable energy sources (RES), namely solar photovoltaic (PV) panels and wind turbines contributes to a clearer environment [2][3]. Moreover, the power management from RES can be efficiently achieved in a DC grid, due to its high controllability and absence of harmonic currents and reactive power [4][5]. For this reason, a PV-based grid can be implemented, for instance, in fast charging stations, whose energy extracted from solar PV panels is used to not overload the power grid and to charge the electric vehicle batteries [6]–[8]. However, the interface of RES demands efficient power converters to attend the innumerous failures that can occur either in the power converters or in the DC grid [9][10]. Due to

2

this fact, it is a constant challenge for researchers to develop solutions to respond to unavoidable failures [11]. In the presence of failures, the power semiconductors that constitute the power converters, and its drivers are quite vulnerable [12]–[14]. To circumvent those problems caused by the presence of failures in the power converters or in the DC grid, the development of fault-tolerant converters is required [15]. This type of topologies can require additional hardware in order to guarantee the normal operation under fault conditions, avoiding the damage of adjacent hardware [16]–[18]. Due to the necessity of additional hardware, the development of fault-tolerant converters can lead to increased costs, namely sensors to the application of fault diagnostic strategies or the introduction of power semiconductors [19][20]. Despite that, the damage caused by non-fault-tolerant converters can be more expensive and harmful [21].

In this paper, a non-isolated three-level DC-DC converter integrated in a bipolar DC grid is presented. The DC-DC converter is used to interface RES, namely solar PV panels [22] as demonstrated in Fig. 1. The main application of this DC-DC converter is to continuously extract, considering the weather scenarios, the maximum energy from PV panels at each moment. However, the aim of this paper is analyzing the behavior of the three-level DC-DC converter in the presence of failures in the positive, neutral, and negative wires of the bipolar DC grid. Thus, it is proved the fault-tolerance of the DC-DC converter, without adding any electronic components.

The presented paper is organized as follows: In Section 2 are described in detail the operation modes of the non-isolated three-level DC-DC converter in normal conditions and in the presence of a failure in the DC wire. Furthermore, it is described the adopted control strategy to extract energy from the solar PV panels (boost-mode). In Section 3 are discussed the simulations results for steady-state and transient-state operations of the three-level DC-DC converter under normal and fault conditions. Finally, Section 4 presents the main conclusions.
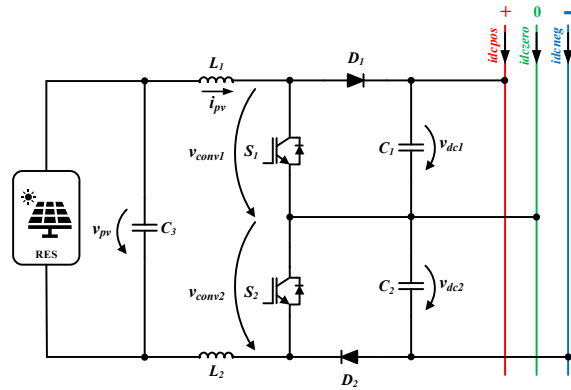

Fig. 1. Electric schematic of the three-level DC-DC converter interfacing solar PV panels connected to a bipolar DC power grid.

2 Operating Principles of the Three-Level DC-DC Converter

This section presents a detailed description of the different operation modes of the three-level DC-DC converter under normal and fault conditions. In normal conditions, there is not any fault in the bipolar DC grid, whereas in fault conditions are presented three possible failures: (a) a failure in the positive wire of the bipolar DC grid; (b) a failure in the neutral wire of the bipolar DC grid; (c) a failure in the negative wire of the bipolar DC grid.

2.1 Operation Modes in Normal Conditions

The presented three-level DC-DC converter integrated in a bipolar DC-DC converter aims to extract the energy from the solar PV panels. The topology demonstrated in Fig. 1 consists of two power semiconductors totally controlled (IGBTs in this case), two diodes, two inductors and a split DC-link. The output voltages, v_{conv1} and v_{conv2}, depend on the states of the semiconductors S_1 and S_2 and the DC-link voltage. In case of the semiconductors S_1 and S_2 are disabled, the current flows through the diodes D_1 and D_2. The value of v_{conv1} is $+v_{dc1}$ and v_{conv2} is $+v_{dc2}$. If the semiconductors S_1 and S_2 are enabled, v_{conv1} and v_{conv2} are zero. When the diode D_1 is directly polarized and the semiconductor S_2 is enabled, v_{conv1} is $+v_{dc1}$ and v_{conv2} is zero. Finally, if S_1 is enabled and D_2 is directly polarized, v_{conv2} assumes the value of $+v_{dc2}$ and v_{conv1} is zero. The values $+v_{dc1}$ and $+v_{dc2}$ corresponds to $+v_{dc}/2$ since the capacitors C_1 and C_2 of the DC-link are equal.

2.2 Operation Modes in Fault Conditions

As mentioned previously, the three-level DC-DC converter is connected to a bipolar DC grid composed by three wires (positive, neutral and negative wires), where can occur failures in those wires of the DC grid. In this section is described the different operation modes of the DC-DC converter under fault conditions. Fig. 2 demonstrates the operating modes of the DC-DC converter under a failure in the positive wire. As it can be observed, the DC-DC converter presents two different operation modes. In case of the current value from PV panels, i_{pv}, presents a lower value than the reference current, i_{pv} flows through the semiconductor S_1 and the diode D_2 (Fig. 2(a)), otherwise i_{pv} flows through the semiconductors S_1 and S_2 (Fig. 2(b)). For both cases, the diode D_1 is not conducting due to the presence of a failure in the positive wire, as well as the voltage in capacitor C_1 is zero. Despite the failure in the positive wire in the DC grid, the DC-DC converter operates in boost-mode, as it is intended.

Fig. 3 shows the operations modes of the three-level DC-DC converter under a failure in the neutral wire. When i_{pv} is lower than the reference current, the current flows through the diodes D_1 and D_2 and the capacitors C_1 and C_2 (Fig. 3(a)). Thus, the inductors store the energy until reaching the intended current. Otherwise, i_{pv} flows through the semiconductors S_1 and S_2 (Fig. 3(b)). Depending on the value of i_{pv} according to its reference, the voltage v_{conv1} assumes the value $+v_{dc}$ which corresponds to the sum of the voltage v_{dc1} with the voltage v_{dc2} or the value zero.
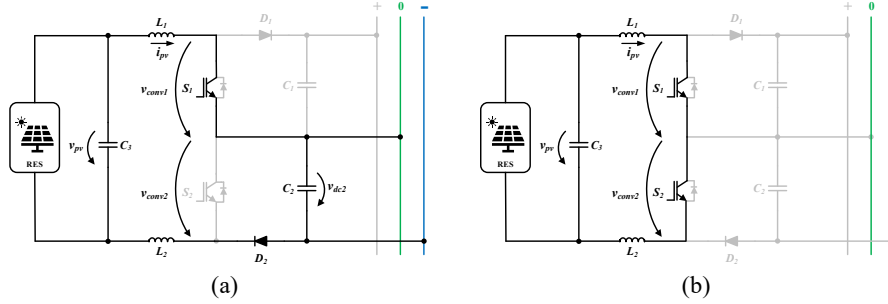
Fig. 2. Operating principles of the three-level DC-DC converter under a failure in the positive wire of the bipolar DC power grid: (a) $v_{conv1} = 0$ and $v_{conv2} = +v_{dc2}$; (b) $v_{conv1} = 0$ and $v_{conv2} = 0$.
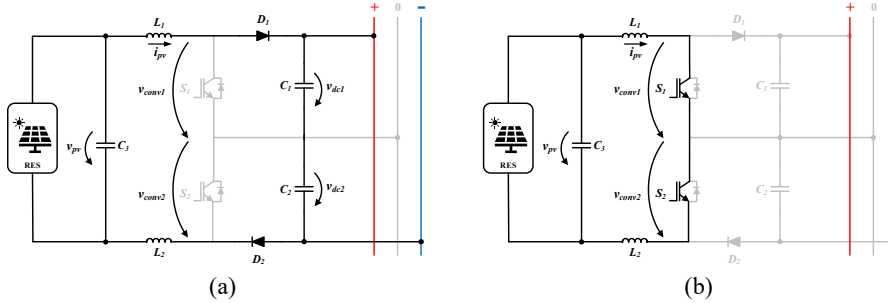

Fig. 3. Operating principles of the three-level DC-DC converter under a failure in the neutral wire of the bipolar DC power grid: (a) $v_{conv1} = +v_{dc}$ and $v_{conv2} = 0$; (b) $v_{conv1} = 0$ and $v_{conv2} = 0$.

Fig. 4 presents the operating principles of the three-level DC-DC converter in the presence of a failure in the negative wire of the DC grid. In this case, the output voltage v_{conv1} assumes the value $+v_{dc1}$ or zero and v_{conv2} is zero. Depending on the current value in the inductors relatively to the reference current, there are two possible operation modes. Fig. 4(a) shows the operation mode when i_{pv} is lower than the established reference current, where the current from the PV panels flows through D_1 and S_2. When i_{pv} is higher than the reference current, the current flows through the semiconductors S_1 and S_2, as demonstrated in Fig. 4(b).
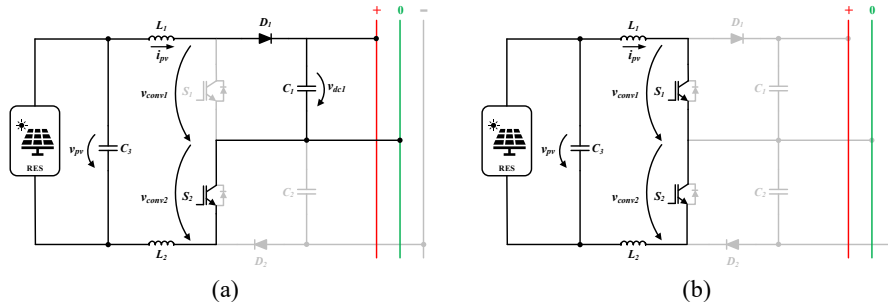

Fig. 4. Operating principles of the three-level DC-DC converter under a failure in the negative wire of the bipolar DC power grid: (a) $v_{conv1} = +v_{dc1}$ and $v_{conv2} = 0$; (b) $v_{conv1} = 0$ and $v_{conv2} = 0$.

For both situations (normal and fault conditions) the control strategy applied to the three-level DC-DC converter is presented through expression (1). The voltages to be synthetized by the three-level DC-DC converter correspond to v_{cv_dc1} and v_{cv_dc2}. On the other hand, the voltage in the solar PV panels is presented by v_{pv} and $i_{Lx}[k]$ is the current in inductor L_1 or L_2 at instant $[k]$. The established reference current that the DC-DC converter must synthetize corresponds to the parameter $i_{Lx}[k + 1]$ at instant $[k + 1]$.

$$v_{cv\_dcx} = v_{pv} - (L_1 + L_2)\,f\,(i_{Lx}[k + 1] - i_{Lx}[k]), \quad x = \{1, 2\} \tag{1}$$

where f is the sampling frequency.

The comparison between v_{cv_dc1} and v_{cv_dc2} with two triangular carriers phase shifted 180º, results in the control signals of semiconductors S_1 and S_2.

3   Simulations of the Three-level DC-DC Converter

In this section are described the simulation results of the three-level DC-DC converter carried out with the software PSIM. The presented simulation results include the steady-state and transient-state operations in two different scenarios: normal conditions and fault conditions. It is used a voltage source of 100 V to emulate the solar PV panels, since the aim of this paper is the fault analysis of the DC-DC converter, and the maximum power tracking control of PV panels is not in the scope of this paper. Moreover, it is considered a voltage value of 200 V in each DC-link capacitor. The DC-link capacitors, C_1 and C_2, assume a capacitance value of 8.2 mF and the inductors L_1 and L_2 have an inductance value of 1.2 mH.

3.1   Steady-State Operation: Normal and Fault Conditions

Fig. 5 shows the steady-state operation of the three-level DC-DC converter in normal conditions, i.e., in the absence of any failure in the DC grid. In this case, it is established a reference current of 10 A. As it can be observed, the ripple frequency of i_{pv} is 40 kHz, which corresponds to the double of the switching frequency (20 kHz). As the DC-DC converter is operating in normal conditions, the voltages synthesized by the DC-DC converter, v_{conv1} and v_{conv2}, can assume the voltage values of zero and $+v_{dc}/2$ (200 V). Thus, when the semiconductors S_1 and S_2 are enabled, v_{conv1} and v_{conv2} is zero. If S_1 is enabled and S_2 is disabled, v_{conv2} is 200 V and v_{conv1} is 0 V, otherwise v_{conv2} is 0 V and v_{conv1} is 200 V. In this case, the duty-cycle of S_1 and S_2 is 75%, whose command signals are the result of the comparison with two triangular carriers of 20 kHz 180º phase shifted, resulting in the voltages v_{conv1} and v_{conv2}.

Fig. **6** presents the steady-state operation of the three-level DC-DC converter in normal and fault conditions in the positive wire for a reference current of 8 A. Initially, the three-level DC-DC converter is operating normally until time instant 0.004 s, when a failure occurs in the positive wire of the bipolar DC grid. In the presence of the failure, it can be observed that the ripple frequency of i_{pv} is half the frequency (20 kHz) verified in normal conditions (40 kHz). Since there is a failure in the posi-

6

tive wire of the bipolar DC grid, there is no energy in capacitor C_1, so the current never flows through the diode D_1 and the energy from the PV panels is not injected into the positive wire of the bipolar DC grid. Thus, v_{conv1} is 0 V and v_{conv2} can assume the values 0 V and 200 V. Due to this, the semiconductor S_1 is always enabled, and the duty-cycle of S_2 is reduced from 75% to 50% to maintain the current value according to its reference. As voltage v_{conv1} is zero, the ripple of i_{pv} is higher than the current ripple verified for normal conditions. The two possible operation modes for this case are presented in Fig. 2.

Fig. 7 shows the steady-state operation of the three-level DC-DC converter in normal and fault conditions in the neutral wire of the bipolar DC grid, for a reference current of 6 A. The three-level DC-DC converter is operating in normal conditions until time instant 0.008 s. However, in the presence of a failure in the neutral wire of the bipolar DC grid, the ripple frequency of i_{pv} changes from 40 kHz to 20 kHz, as observed in the previous case. Moreover, v_{conv1} assumes the values 0 V and 400 V, whose last value corresponds to the total voltage value of the DC-link, whereas v_{conv2} is 0 V. On the other hand, as v_{conv2} assumes the value 0 V the ripple of i_{pv} is higher than the current ripple verified in normal conditions. In the presence of a failure in the neutral wire, both semiconductors S_1 and S_2 switch and the current flows through D_1 and D_2, resulting in the operation modes presented in Fig. 3.
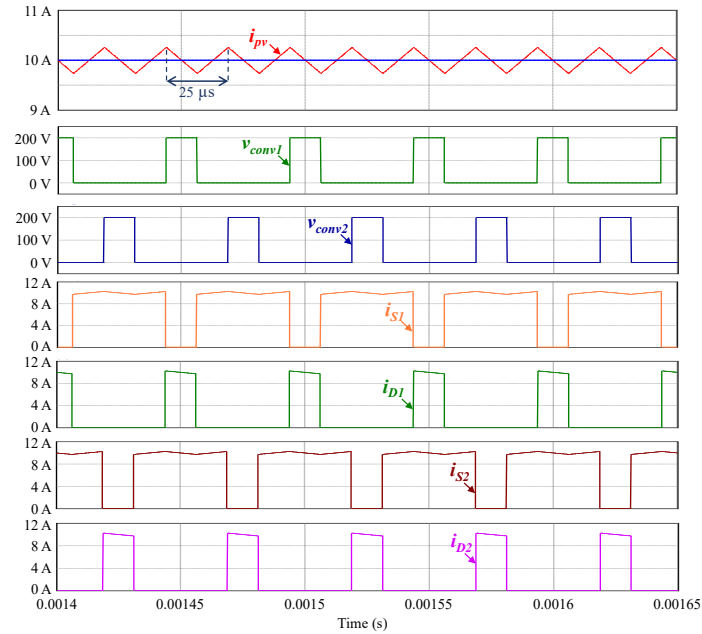

Fig. 5. Steady-state operation of the three-level DC-DC converter in normal conditions for a reference current of 10 A.
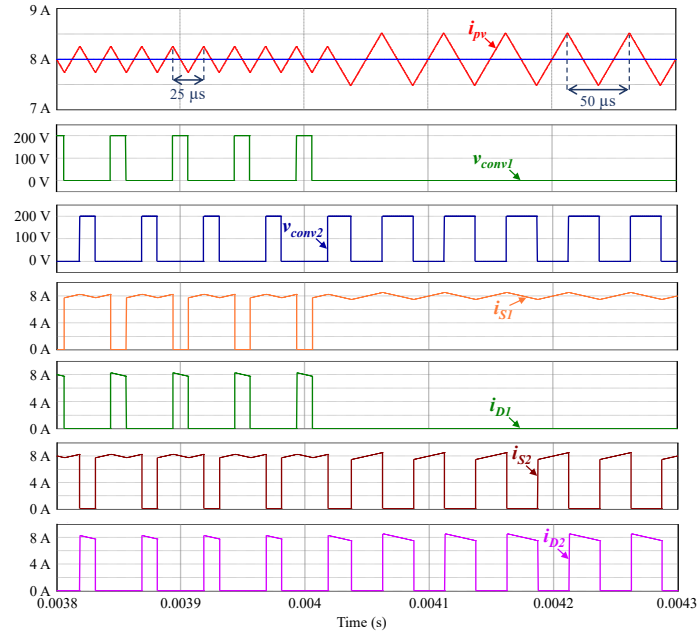
Fig. 6. Steady-state operation of the three-level DC-DC converter in normal and fault conditions in the positive wire for a reference current of 8 A.

Fig. 8 presents the steady-state operation of the three-level DC-DC converter in normal and fault conditions in the negative wire of the bipolar DC grid, for a reference current of 4 A. As the previous case, the ripple frequency of i_{pv} in the presence of a failure in the bipolar DC grid, changes from 40 kHz to 20 kHz. Due to the presence of a failure in the negative wire of the bipolar DC grid, there is no energy in C_2 and the energy from the PV panels is not injected into the negative wire of the bipolar DC grid, so the current in D_2, i_{D2}, is 0 A. For this reason, v_{conv2} is 0 V and v_{conv1} can assume the values 0 V and 200 V. As voltage v_{conv2} is 0 V, the ripple of i_{pv} is higher than the current ripple verified for normal conditions. Furthermore, the semiconductor S_2 is always enabled, and the duty-cycle of S_1 is reduced from 75% to 50% in order to maintain the current value according to its reference. The two possible operation modes for this case are presented in Fig. 4.
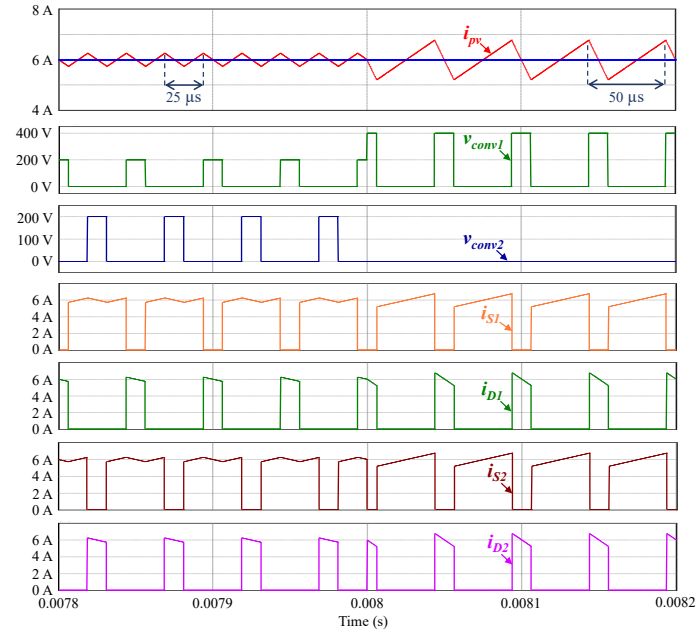
8

Fig. 7. Steady-state operation of the three-level DC-DC converter in normal and fault conditions in the neutral wire for a reference current of 6 A.
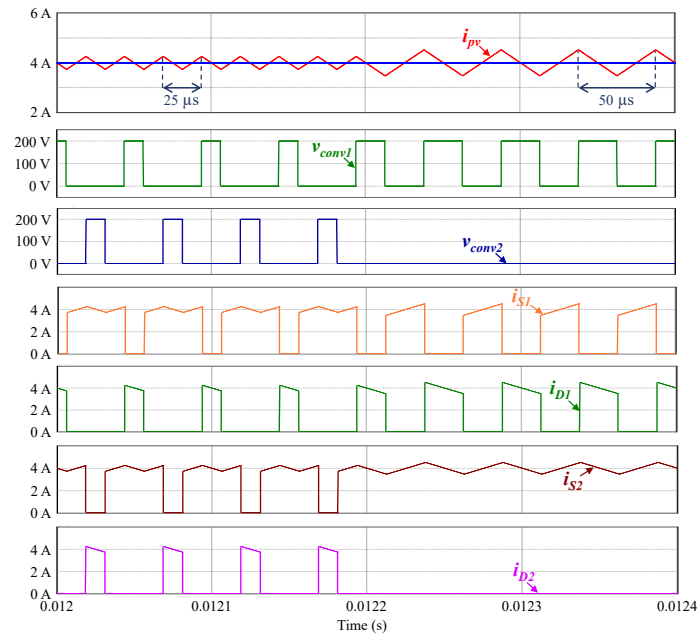

Fig. 8. Steady-state operation of the three-level DC-DC converter in normal and fault conditions in the negative wire for a reference current of 4 A.

3.2 Transient-State Operation: Normal and Fault Conditions

Fig. 9 illustrates the transient-state operation of the three-level DC-DC converter in normal conditions. Initially, the reference current is 10 A and it is reduced to 8 A at time instant 0.002 s. In this case, the transition time takes 25 µs. Moreover, the ripple frequency of i_{pv} is 40 kHz, i.e., the double of the switching frequency. As the three-level DC-DC converter is operating in normal conditions, the output voltages, v_{conv1} and v_{conv2}, assume the values 0 V and 200 V. When S_1 and S_2 are enabled, v_{conv1} and v_{conv2} are zero. If S_1 is enabled and S_2 is disabled, v_{conv2} is 200 V and v_{conv1} is 0 V, otherwise v_{conv2} is 0 V and v_{conv1} is 200 V. The duty-cycle of S_1 and S_2 is 75%.

Fig. 10 shows the transient-state operation of the three-level DC-DC converter in the presence of a failure in the positive wire of the bipolar DC grid. At time instant 0.0055 s the reference current is reduced to 6 A, whose transition time is 50 µs. The transition time verified is higher than in normal conditions (25 µs). Moreover, the ripple of i_{pv} is the same verified in fault conditions, i.e., the ripple is higher than in normal conditions. This is since the output voltage v_{conv1} is 0 V, where S_1 is always enabled and there is no energy injected into the positive wire of the bipolar DC grid. So, i_{D1} is 0 A and the current flows through S_1 and S_2 or S_1 and D_2.
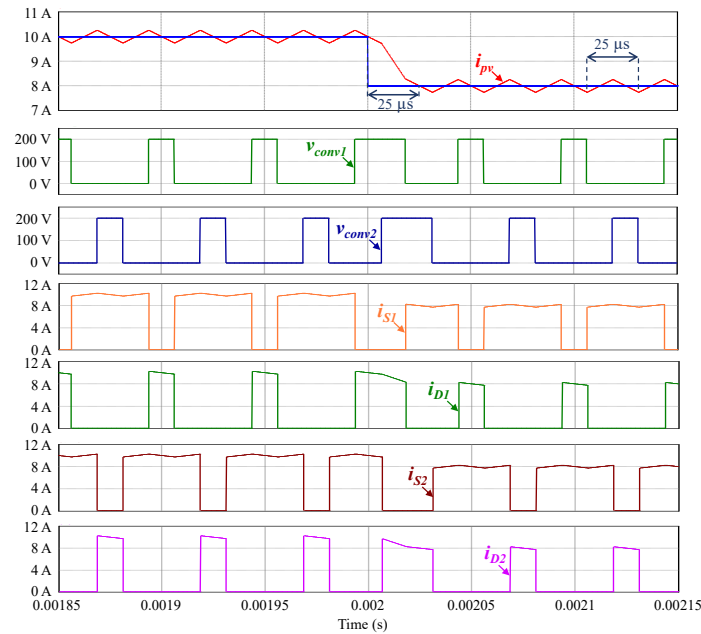

Fig. 9. Transient-state operation of the three-level DC-DC converter in normal conditions for reference currents of 10 A and 8 A.
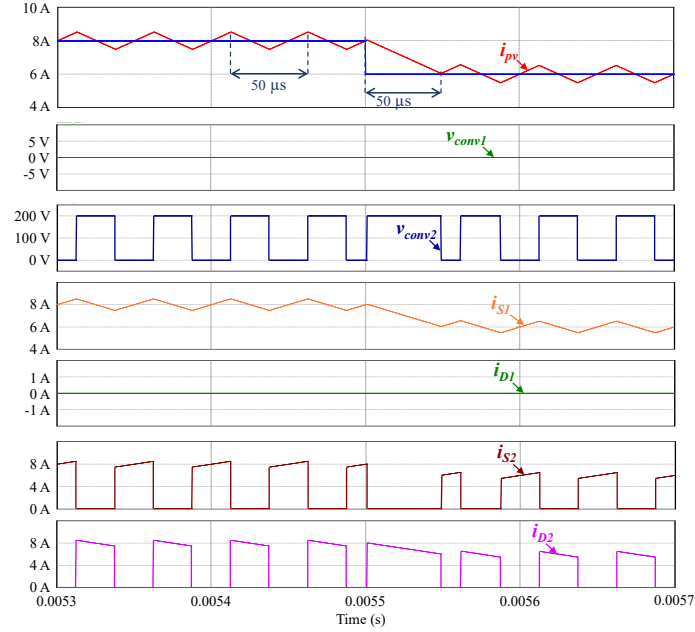
Fig. 10. Transient-state operation of the three-level DC-DC converter in the presence of a failure in the positive wire of the DC power grid for reference currents of 8 A and 6 A.

Fig. 11 presents the transient-state operation of the three-level DC-DC converter in the presence of a failure in the neutral wire of the bipolar DC grid. Initially, the established reference current is 6 A and at time instant 0.0095 s the reference current is reduced to 4 A, whose transition time took 25 µs. As mentioned above, in the presence of a failure in the neutral wire of the bipolar DC grid, v_{conv1} assumes the values 0 V and 400 V and v_{conv2} is 0 V. As v_{conv2} is null, the ripple of i_{pv} is higher than the current ripple verified in normal conditions.

Fig. 12 illustrates the transient-state operation of the three-level DC-DC converter in the presence of a failure in the negative wire of the bipolar DC grid. At time instant 0.0135 s the reference current changes from 4 A to 2 A, whose transition time is 50 µs. In the presence of a failure in the negative wire of the bipolar DC grid, v_{conv1} assumes the values 0 V and 200 V and v_{conv2} the value 0 V. In this case, the energy is injected from the PV panels into the bipolar DC grid, through the semiconductors S_2 and S_1 or S_2 and D_1.

Despite the presence of failures in the positive, neutral or negative wire of the bipolar DC grid, i_{pv} follows correctly the reference current.
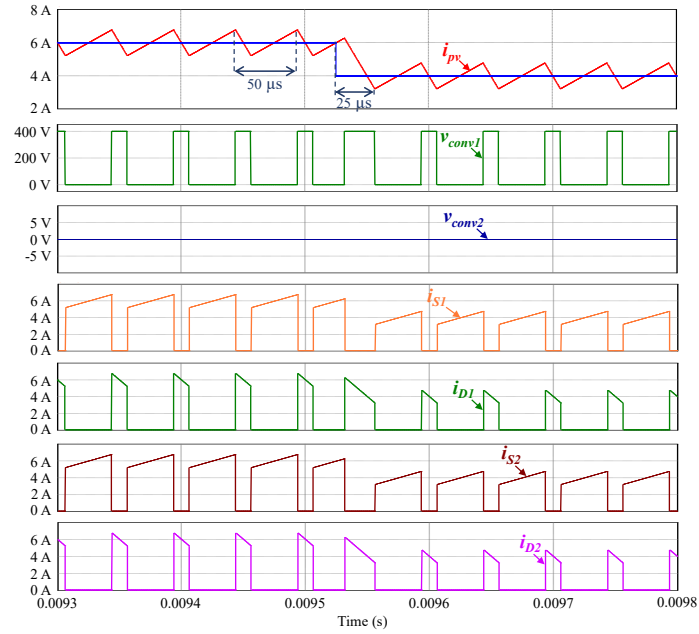
Fig. 11. Transient-state operation of the three-level DC-DC converter in the presence of a failure in the neutral wire of the DC grid for reference currents of 6 A and 4 A.
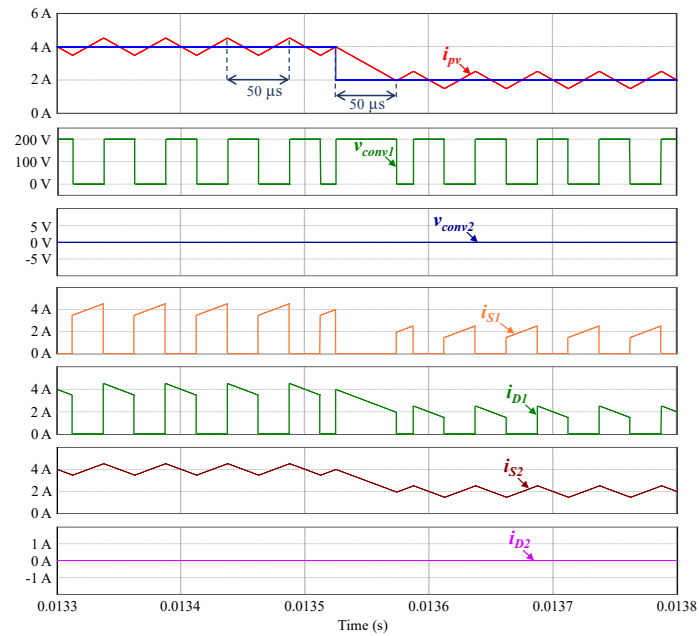

Fig. 12. Transient-state operation of the three-level DC-DC converter in the presence of a failure in the negative wire of the DC power grid for reference currents of 4 A and 2 A.

4   Conclusions

In this paper, a three-level DC-DC converter is analyzed in normal and fault conditions connected to a bipolar DC power grid. The three-level DC-DC converter aims to interface solar photovoltaic (PV) panels into a bipolar DC power grid. The presented DC-DC converter is analyzed in normal conditions considering steady-state and transient-state operations. The results are compared with the DC-DC converter operating in the presence of a failure, individually, in the positive, neutral and negative wires of the DC grid. Moreover, the validation was performed for different values of the reference currents. It is demonstrated that, despite the presence of failures in the bipolar DC grid, the current from the PV panels, i_{pv}, correctly follows the established reference current. However, the ripple of i_{pv} is higher in presence of failures than in normal operating conditions, but analyzing the presented simulation results, this aspect is not critical. As shown, the three-level DC-DC converter presents good results in normal and in the fault conditions reported in this paper, without compromising the power extraction from the solar PV panels.

Acknowledgment

References

[1]   J. Li, X. Zhang, S. Ali, and Z. Khan, "Eco-innovation and energy productivity: New determinants of renewable energy consumption," *Journal of Environmental Management*, vol. 271, p. 111028, 2020.

[2]   O. J. Akintande, O. E. Olubusoye, A. F. Adenikinju, and B. T. Olanrewaju, "Modeling the determinants of renewable energy consumption: Evidence from the five most populous nations in Africa," *Energy*, vol. 206, p. 117992, 2020.

[3]   M. Ahmed, S. Kuriry, M. Shafiullah, and M. Abido, "DC Microgrid Energy Management with Hybrid Energy Storage Systems," in *2019 23rd International Conference on Mechatronics Technology (ICMT)*, pp. 1–6, 2019.

[4]   H. Matayoshi, M. Kinjo, S. S. Rangarajan, G. G. Ramanathan, A. M. Hemeida, and T. Senjyu, "Islanding operation scheme for DC microgrid utilizing pseudo Droop control of photovoltaic system," *Energy for Sustainable Development*, vol. 55, pp. 95–104, 2020.

[5]   S. Cui, J. Hu, and R. De Doncker, "Fault-Tolerant Operation of a TLC-MMC Hybrid DC-DC Converter for Interconnection of MVDC and HVdc Grids," *IEEE Transactions on Power Electronics*, vol. 35, no. 1, pp. 83–93, 2019.

[6]   D. Wang, F. Locment, and M. Sechilariu, "Modelling, Simulation, and Management Strategy of an Electric Vehicle Charging Station Based on a DC Microgrid," *Applied Sciences*, vol. 10, no. 6, p. 2053, 2020.

[7]   M. Sechilariu, N. Molines, G. Richard, H. Martell-Flores, F. Locment, and J. Baert, "Electromobility framework study: infrastructure and urban planning for EV charging station empowered by PV-based microgrid," *IET Electrical Systems in Transportation*, vol. 9, no. 4, pp. 176–185, 2019.

[8]   V. Monteiro, J. G. Pinto, and J. L. Afonso, "Experimental validation of a three-port integrated topology to interface electric vehicles and renewables with the electrical grid," *IEEE Transactions on Industrial Informatics*, vol. 14, no. 6, pp. 2364–2374, 2018.

[9]   V. Monteiro, N. Tashakor, T. J. Sousa, T. Kacetl, S. Götz, and J. L. Afonso, "Review of Five-Level Front-End Converters for Renewable-Energy Applications," *Frontiers in Energy Research*, vol. 8, p. 172, 2020.

[10]   A. B.-B. Abdelghani, J. Sakly, H. B. Abdelghani, and I. Slamabelkhodja, "Reliable, efficient and fault tolerant power converter for grid-connected PV system," in *2018 International Conference on Electrical Sciences and Technologies in Maghreb (CISTEM)*, pp. 1–6, 2018.

[11]   S. Csaba and S. Razvan, "Transient Phenomena and Failures Analysis in Redundant Power Converters," in *2019 8th International Conference on Modern Power Systems (MPS)*, pp. 1–6, 2019.

[12]   F. Bento and A. J. M. Cardoso, "A comprehensive survey on fault diagnosis and fault tolerance of DC-DC converters," *Chinese Journal of Electrical Engineering*, vol. 4, no. 3, pp. 1–12, 2018.

[13]   H. Wen, J. Li, H. Shi, Y. Hu, and Y. Yang, "Fault Diagnosis and Tolerant Control of Dual-Active-Bridge Converter with Triple-Phase-Shift Control for Bidirectional EV Charging Systems," *IEEE Transactions on Transportation Electrification*, 2020.

[14]   K. Hu, Z. Liu, Y. Yang, F. Iannuzzo, and F. Blaabjerg, "Ensuring a reliable operation of two-level IGBT-based power converters: A review of monitoring and fault-tolerant approaches," *IEEE Access*, vol. 8, pp. 89988–90022, 2020.

[15]   V. F. Pires, A. Cordeiro, D. Foito, A. J. Pires, J. Martins, and H. Chen, "A multilevel fault-tolerant power converter for a switched reluctance machine drive," *IEEE Access*, vol. 8, pp. 21917–21931, 2020.

[16]   K. Bi, Q. An, J. Duan, L. Sun, and K. Gai, "Fast Diagnostic Method of Open Circuit Fault for Modular Multilevel DC/DC Converter Applied in Energy Storage System," *IEEE Transactions on Power Electronics*, vol. 32, no. 5, pp. 3292–3296, 2017.

[17]   H. Givi, E. Farjah, and T. Ghanbari, "Switch and Diode Fault Diagnosis in Nonisolated DC–DC Converters Using Diode Voltage Signature," *IEEE Transactions on Industrial Electronics*, vol. 65, no. 2, pp. 1606–1615, 2018.

[18]   E. Farjah, H. Givi, and T. Ghanbari, "Application of an Efficient Rogowski Coil Sensor for Switch Fault Diagnosis and Capacitor ESR Monitoring in Nonisolated Single-Switch

DC–DC Converters," *IEEE Transactions on Power Electronics*, vol. 32, no. 2, pp. 1442–1456, 2017.

[19] G. K. Kumar and D. Elangovan, "Review on fault-diagnosis and fault-tolerance for DC-DC converters," *IET Power Electronics*, vol. 13, no. 1, pp. 1–13, 2020.

[20] S. Zhuo, L. Xu, A. Gaillard, Y. Huangfu, D. Paire, and F. Gao, "Robust open-circuit fault diagnosis of multi-phase floating interleaved DC-DC boost converter based on sliding mode observer," *IEEE Transactions on Transportation Electrification*, vol. 5, no. 3, pp. 638–649, 2019.

[21] F. Bento and A. J. M. Cardoso, "Open-circuit fault diagnosis in interleaved DC-DC boost converters and reconfiguration strategy," in *2017 IEEE 11th International Symposium on Diagnostics for Electrical Machines, Power Electronics and Drives (SDEMPED)*, pp. 394–400, 2017.

[22] A. Rodrigues, C. Oliveira, T. J. C. Sousa, L. Machado, J. L. Afonso, and V. Monteiro, "Unified Three-Port Topology Integrating a Renewable and an Energy Storage System with the Grid-Interface Operating as Active Power Filter," in *2020 IEEE 14th International Conference on Compatibility, Power Electronics and Power Engineering (CPE-POWERENG)*, vol. 1, pp. 502–507, 2020.